Multiple-Beam Scanning Electron Microscopy

Anna Lena Eberle,[1]* Richard Schalek,[2] Jeff W. Lichtman,[2] Matt Malloy,[3] Brad Thiel,[4] and Dirk Zeidler[1]

[1]Carl Zeiss Microscopy GmbH, Carl-Zeiss-Str. 22, D-73447 Oberkochen, Germany
[2]Department of Molecular and Cellular Biology, Harvard University, 52 Oxford Street, Cambridge, MA 02138
[3]SEMATECH, 257 Fuller Rd, Suite 2200, Albany, NY 12203
[4]SUNY Polytechnic Institute, 257 Fuller Road, Albany, NY 12203

*anna-lena.eberle@zeiss.com

Introduction

When resolving structures at nanometer scale, electron microscopes are the tools of choice. Since the invention of the electron microscope, the technology has matured into a standard technique applied in a wide variety of disciplines and laboratories. This holds especially true for scanning electron microscopes (SEMs), which have developed from room-filling equipment operated by highly specialized scientists to automated, desktop-sized, or even mobile, tools [1].

Some of the major advancements of SEMs in recent years have been (a) increases in resolution, especially at low electron landing energies [2]; (b) improvements in usability through digitalization, advances in software and tool handling, or miniaturization [3]; (c) addition of improved detection schemes such as energy- or wavelength-dispersive X-ray spectrometry (EDX, WDX) to maximize the amount of information that can be taken from the sample [4]; and (d) combinations of electron microscopy with other microscopic techniques for correlative microscopy [5–9]. SEMs have become ubiquitous tools that are used in various environments and for many different applications; they no longer require highly specialized operators. For many SEM applications in practice, the highest achievable resolution is not required [10].

There is one aspect of SEM performance that has not yet been improved significantly: the speed with which micrographs of a sample are acquired while maintaining both nanometer resolution and high signal-to-noise ratio (SNR). As a result, high-resolution SEM images can be obtained in a reasonable amount of time only from small areas. Up to now, this has not been much of an impediment to SEM applications, as need for high-throughput electron microscopy at high resolution has been confined to relatively few fields. This situation, however, is changing; the next paragraphs describe three examples.

Wafer defect detection. With the continuing decrease of structure size in semiconductors, there is a need for detection of particles or pattern defects that are now only a few nanometers in diameter. Quality control of wafers with light optical techniques is becoming increasingly challenging because the particle sizes leading to a defect have become much smaller than the light wavelengths employed [11]. Detecting these particles or pattern defects with an SEM [10] requires that large areas be scanned for features at nanometer resolution. Currently, due to throughput limitations, SEMs cannot be used to map whole wafers at high resolution: in theory, scanning a complete 300 mm wafer at, say, 10 nm pixel size and 20 MHz data acquisition rate (equivalent to 50 ns dwell time per pixel), would result in a lower limit of about 1 year of acquisition time, not taking into account the overhead time. Therefore, today, SEMs can be used to sample only a statistically significant fraction of the wafer area. Increasing the fraction of the scanned sample area will reduce the number of "false negative" events, that is, critical defects that were missed.

Imaging organ tissue. Similarly, many medical investigations of histological samples with electron microscopes follow a protocol wherein a number of sample positions are screened for special indicators [12]. Here, reducing "false negative" events is of vital interest. Imaging whole organs and tissues that exhibit particular architectures, wherein the assembly of structure from cell scale to large scale follows hierarchical patterns [13–14], is an important task that up to now required different imaging methods for bridging the gaps between different length scales. Imaging these structures within one electron microscope would greatly improve functional inferences across length scales.

Volume imaging. For imaging biological samples with electron microscopy, there is an increasing need to image large volumes of biological tissue at high resolution to gain insight into the functioning of parts of organs or even whole organs. Examples include the understanding of neural circuits [15–16] and the analysis of extended cellular structures [17]. The resolution that is required to obtain information at a sufficiently detailed level can only be obtained by electron microscopy. Using SEMs to this end currently results in data acquisition rates too low to accommodate even modestly sized volumes. For example, imaging a block of tissue of 2 mm side length with an isotropic voxel size of 10 nm would result in about 8 Petabytes (PB) of data. At a data acquisition rate of 20 MHz, this would require a total acquisition time of about 12 years, even before taking into account overhead times such as the time needed to move the sample between the scans.

All three of the above-mentioned application examples show that there is a need for imaging large areas or volumes at high resolution with high-throughput electron microscopes. In this article, we demonstrate a throughput increase of more than one order of magnitude with a multi-beam SEM.

Materials and Methods

How does a multi-beam SEM work? The multi-beam SEM uses multiple electron beams in one electron optical column and one detector for each beam. A diagram of the system layout is shown in Figure 1. A multi-beam electron source produces an array of electron beams that are subsequently focused onto the

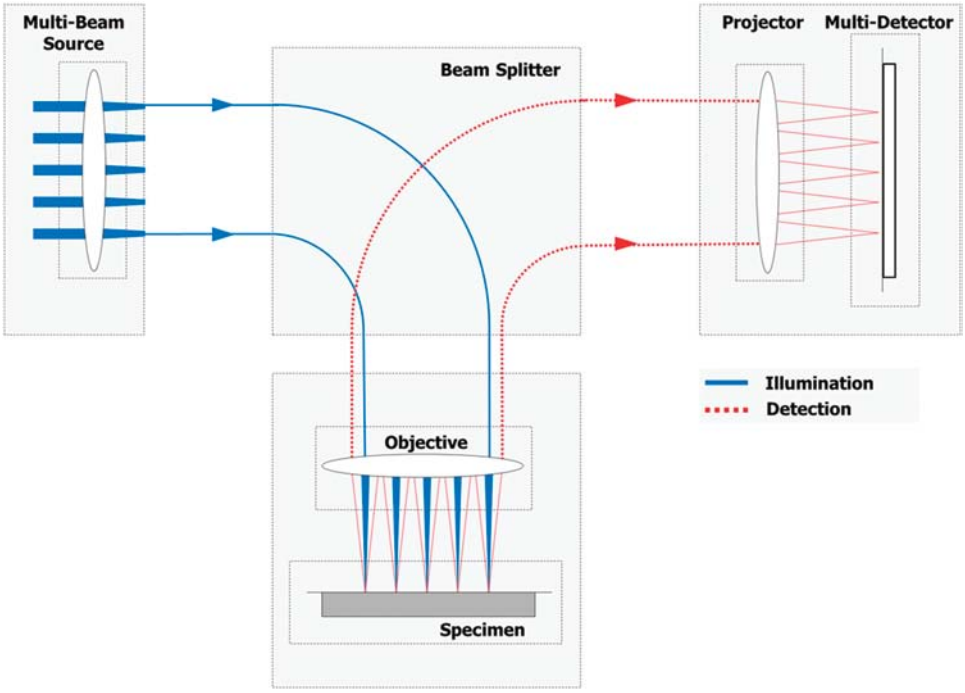

Figure 1: Schematic diagram of the multi-beam SEM setup. Primary electrons (solid lines, blue) are focused onto the sample and separated by a beam splitter from the secondary electrons (dotted lines, red) that are detected simultaneously. The separate electron beams form many individual images, which are then merged into a single large-area image as shown in Figure 2.

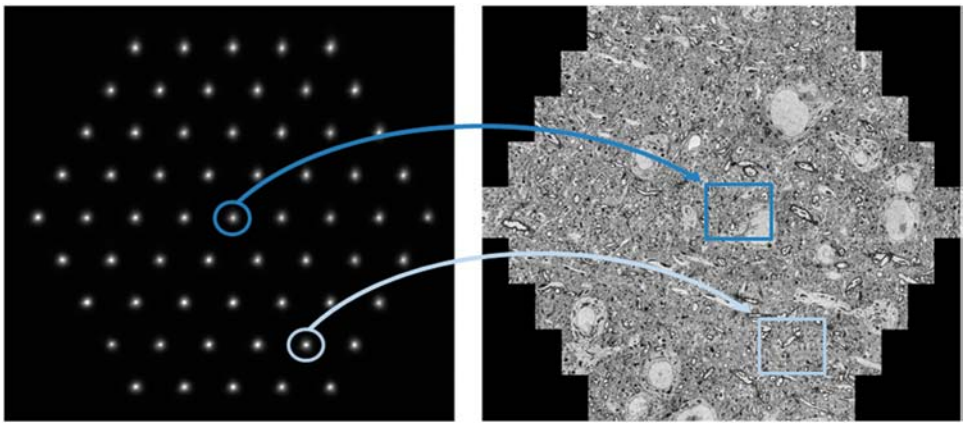

Figure 2: Multi-beam SEM principle of operation. The left image shows the 61 secondary electron spots at the detector plane. Each spot corresponds to one emitted secondary electron beam acquired by one detector. All beams are scanned concurrently. As an example, the beams marked in dark and light blue simultaneously acquire the images marked in dark and light blue, respectively. The right image shows a montage of the 61 single-beam images recorded in one shot with a total FOV of about 110 µm. (Tissue sample by Jeff Lichtman and Richard Schalek, Harvard University.)

sample. The primary beams are arranged in a hexagonal pattern to minimize electron optical aberrations. Secondary electrons emanating from each primary electron spot are imaged onto a multi-detector with one detection unit for each electron beam. A magnetic beam splitter separates primary and secondary electron beams. Figure 2 shows the principle of operation. The 61 electron beams are scanned over the sample with one global scanner, and a secondary electron signal is acquired for each scan position of each beam. A complete image of the region underneath the primary beam array is thus obtained in the time it takes one beam to scan its small sub-area. With this parallelization, data acquisition can be sped up by a factor of 61, if 61 beams are used, and even higher for more beams. The data acquisition system also must be highly parallelized to accommodate the large data acquisition rates with our current comparably low-bandwidth data transfer and storage solutions.

Why multi-beam instead of single beam? To make a specific data set such as an SEM image recognizable to a human being, features in the data set must be sufficiently visible against the ubiquitous background of noise [18]. Because the analysis of large image data sets of several Terabytes or even Petabytes is difficult if not impossible for human beings, automated image processing by computers is required. Again, to make a data set evaluable to an algorithm, the features of interest must be detectable against background noise [19]. In other words, the SNR of the image must be sufficiently high.

In a real-world situation, noise is present in most steps of the SEM image generation process and will contribute to the noise content in the image, such as shot noise caused by the fact that electric charges are quantized and thermal noise that originates from electronic circuits in any SEM detection path. If fast data acquisition rates are needed, the limiting noise term will be shot noise of the electrons impinging onto the sample. The signal-to-noise ratio for shot noise is proportional to $\sqrt{N}$, where N is the number of electrons used to illuminate one pixel. This electron dose is determined by the pixel dwell time and the beam current. On the other hand, signal amplitude is given by the contrast of the sample, that is, the electron yield difference at different locations of the sample, and the fraction of electrons emanating from the sample that is detected, that is, the detection efficiency. Methods to enhance SNR include enhancing contrast by optimizing the staining procedure and detecting as many signal electrons as possible.

Another important specification is the size of the electron beam that probes the sample. If the probe size is too large for the size of the features that are to be imaged, the reconstructed image, being a convolution of the sample structure with the shape of the electron beam profile, will be smeared out, such that the desired features will no longer be detectable.

Hence, the maximum achievable scan speed of any conventional SEM is ultimately limited by the electron

dose per pixel required to generate a desired minimal SNR at a given spot size. In conventional electron microscopic imaging, the goal is usually to obtain the optimal resolution and optimal contrast for all images, with a beam size clearly smaller than the feature size. In high-throughput electron microscopy, beam size, scan pixel size, and electron dose per pixel all have to be chosen such that a good-enough SNR is achieved at the maximum data acquisition rate. It should be noted that, for wafer inspection, SNR might be sacrificed for throughput even more than in imaging applications, as it is sufficient to flag the general location of a pattern defect to be reviewed later with higher fidelity.

Two fundamental effects limit the maximum scan speed, or minimum pixel dwell time, of single-beam SEMs. First, reducing dwell time per pixel while retaining SNR requires increasing the beam current, which ultimately leads to increasing Coulomb interactions between the electrons, thereby blurring the electron beam and reducing the resolution at the sample. Second, efficient detectors for secondary electrons in an SEM cannot be operated faithfully at arbitrarily high rates because of detector decay times. The dwell time per pixel is therefore ultimately limited by the bandwidth of the electron detector.

With multiple electron beams in a single column, Coulomb interactions will be lower than in a single-beam configuration, as the charge is distributed among many beams and therefore spread over a larger volume [20]. Multi-beam configurations therefore maintain high resolution and high total current at the sample at the same time. Having a dedicated detector for each beam bypasses the detector bandwidth limit. The total possible detector bandwidth of the multiple-beam SEM is the single detector bandwidth times the number of beams. With this setup, the multi-beam SEM is prepared for future single-beam SEM detector technology improvements that might feature higher bandwidths per detector. The electron optical design ensures that almost all secondary electrons are guided to the multi-detector to obtain the best possible SNR at a given primary beam current. This is equivalent to, for a given SNR and electron beam parameters, the efficient use of primary electrons to generate a secondary electron signal resulting in a minimum electron beam damage of the sample.

Results

The multi-beam SEM is compatible with the sample preparation methods for a number of the applications mentioned in the introduction. The figures below give examples of the increase in throughput attained. The multi-beam SEM can typically operate at landing energies of 1–3 keV with an electron probe size to match scan pixel sizes of 4–10 nm and a total current in the range of several tens to several hundreds of nA.

Imaging tissue volumes. The acquisition of volume data from biological tissue with an SEM requires sectioning of the volume, for which several approaches exist [21]. The serial block-face imaging technique employs an ultramicrotome located within the SEM chamber. After the surface of the tissue block is imaged, the microtome knife shaves off the upper tens of nanometers, and the freshly exposed surface is imaged again. This procedure is repeated over and over until a dataset of the entire volume is generated [22]. The main advantage of this technique is a reduced effort for the alignment of the images in the z dimension. The main disadvantage is that the sample is inevitably lost after imaging. A different approach is the collection of a series of ultrathin sections from a standard ultramicrotome on a solid substrate and subsequent imaging with an SEM. This sample preparation method and a device for automated collection of the serial sections are described in [23–24]. The entire experimental setup from sample preparation to imaging strategies is characterized by a high degree of automation to enable the reliable acquisition of large amounts of SEM data [25]. With this approach the samples are preserved for repeated imaging, although the reconstruction effort is greater because of the possible distortion and translation of the sections. In any case, multi-beam imaging has been demonstrated for samples prepared with either approach [26]. As an example, Figure 3 shows several zoomed-in views from an osmium-stained mouse brain section. The sample (Figure 3a) was covered by a mosaic of hexagonal multi-beam fields of view (FOVs) (Figure 3d), each of which consisted of 61 single-beam images (Figure 3e) of sufficient quality for segmentation and further processing. The overview of the complete section (Figure 3a) enables orientation on the basis of anatomical landmarks such as the corpus callosum or the fiber bundles of the subcortical region. By zooming into the dataset (Figures 3b and 3c), it is possible to distinguish individual pyramidal neurons and dendrites, as well as blood vessels. The hexagonal FOV (Figure 3d) forms the basic imaging unit because this is the area imaged in a single scan pass. Enlargements of an individual single-beam image (Figures 3e and 3f), to the limit of native resolution (Figure 3f), show the image quality achievable with a multi-beam SEM. All membranes are clearly visible, and intracellular organelles as mitochondria or endoplasmic reticulum are distinguishable.

Multi-beam acquisition of a volume data set. Figure 4 shows the workflow for a typical volume data acquisition in advance of three-dimensional reconstruction, independent of the method of sample preparation. The workflow is in many aspects similar to the one used with single-beam electron microscopes; that is, the sample is mounted on a stage that moves to a new position after each image acquisition such that the multiple FOVs cover the areas to be inspected.

Tiling images with single-beam SEM. With a single-beam SEM, the images usually have rectangular shape. The relative orientation between the images and the sample is determined by the scan rotation, and can be chosen arbitrarily. An efficient tessellation of the area of interest is possible for any value of the scan rotation because the movement of the stage along the sample dimensions can be chosen to match to the scan rotation such that the area is completely covered with only small overlaps of the FOVs being required. Many sections through the sample are imaged consecutively and finally merged into a three-dimensional data set.

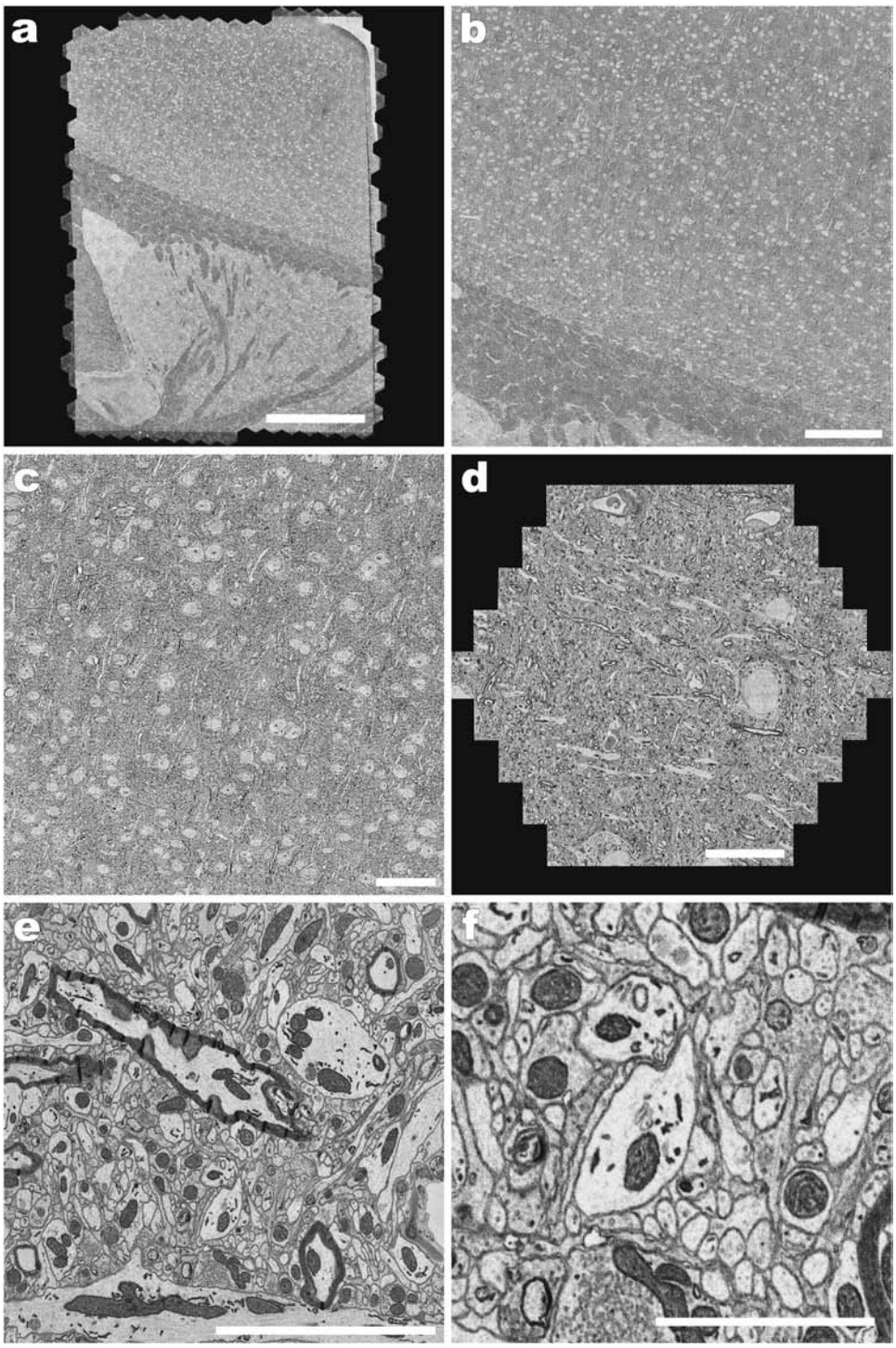

Figure 3: Cortical and subcortical regions of mouse brain hemisphere (serial ultra-thin section), acquired by the multi-beam SEM at 0.45 GPixel/s and 3.8 nm pixel size. (a) Overview image of one complete section generated in a post-processing montage by binning down about 28,000 single-beam images; sample size is 1.5 mm × 2 mm; scale bar is 500 µm. (b)–(f) Details of the data set acquired from (a) with increasing magnification and decreasing binning. Scale bars: (b) 200 µm, (c) 50 µm, (d) 20 µm, (e) 5 µm, and (f) 2 µm. (Sample by Jeff Lichtman and Richard Schalek, Harvard University).

Tiling images with multi-beam SEM. Acquisition of image data with a multiple-beam SEM is performed in the same manner but with a few differences. Here, the tessellation has to consider the relative beam positions of the multiple beams at the sample and the special, hexagonal-like shape of the FOV. For the hexagonal FOV, an overlap-free tiling of the surface is still possible with suitably adapted stage positions. Within a single hexagonal FOV, single-beam images can still be chosen as rectangular in shape for tiling and need not reflect the hexagonal symmetry of the beam pattern. Unlike the single-beam case, the direction of the scan rotation should not be chosen arbitrarily, but rather such that the longer axis of the single images coincides with the direction of one beam to one of its six next neighbors. This minimizes the image size for the single images while maintaining full area coverage. If the scan rotation differs from this beam orientation, a larger image size must be chosen to completely cover the sample area under the multiple beams. This would result in a fraction of the surface being scanned more than once, and, thus, a reduction of throughput. As shown in Figure 4, large *x*-*y* sections from various depths *z* can be merged into a three-dimensional volume data set. Techniques for alignment and reconstruction are similar to those employed by single-beam SEM instruments.

Wafer inspection. The high level of parallelization combined with high resolution that is enabled by this multi-beam configuration is particularly attractive to the semiconductor industry where it is being explored as a way to address critical throughput and sensitivity gaps in wafer inspection. A SEMATECH-led industry program is being established at this time, which will focus on developing and scaling the multi-beam technology to meet high-volume manufacturing requirements for the semiconductor industry. To demonstrate the capabilities of the multi-beam SEM in wafer inspection, Figure 5 shows an image of a test wafer patterned with the SEMATECH AMAG6L reticle that contains test features for metrology experiments, such as line patterns with different nominal line widths and pattern recognition features. The line-to-line spacing in Figure 5 is 60 nm, corresponding to a half pitch of 30 nm. More details about this test wafer can be found in [27]. The workflow here is the same as that for the imaging of a single thin section.

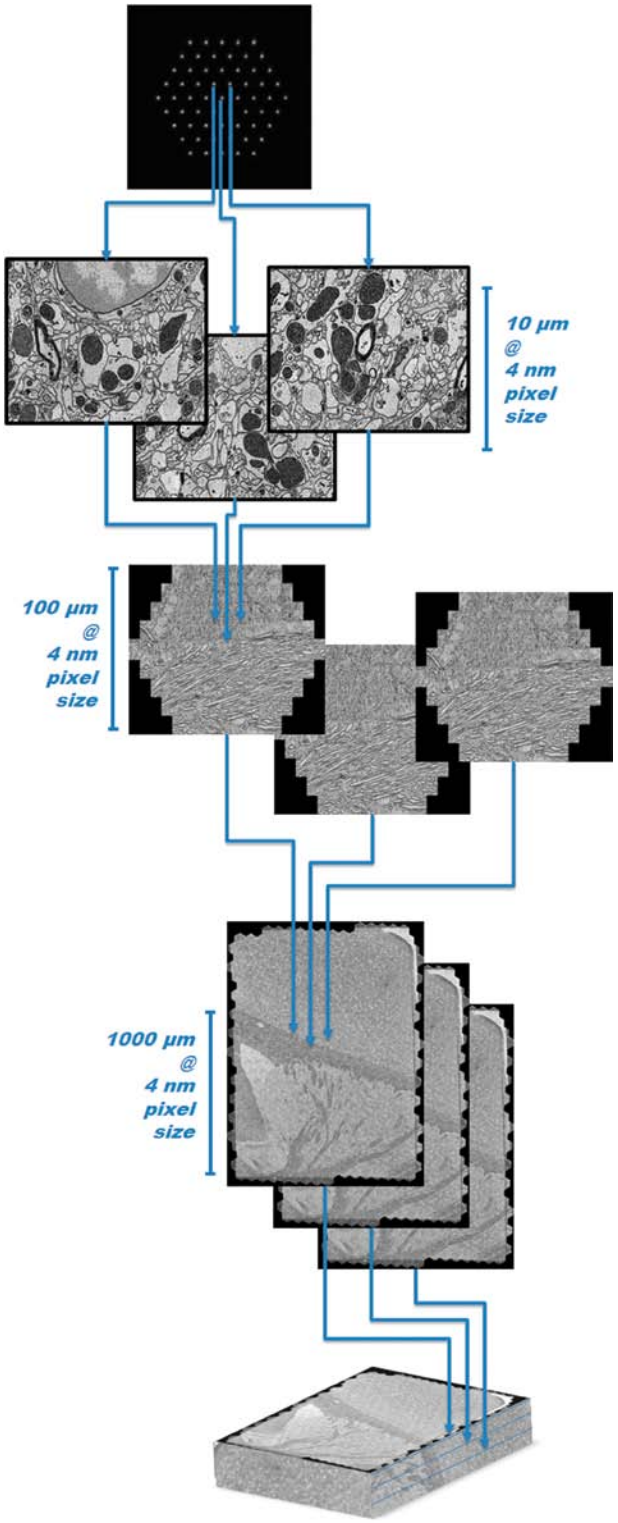

Figure 4: Flow diagram of the workflow for acquiring volumes of tissue, such as brain tissue. The single images corresponding to each beam (upper part, 3 images shown for 3 individual beams) are merged side-by-side into one hexagon of 61 images. The sample is mounted on a stage and moved between acquiring hexagons (middle part, 3 hexagons shown) such that the entire region of interest of one section is imaged. This region of interest is acquired repeatedly for a number of consecutive sections (lower part, 3 sections are shown). After alignment of the 2D image data of all sections perpendicular to the cutting direction and with reference to the features contained within the tissue [25], the image data is cast into a volumetric data set (lower part).

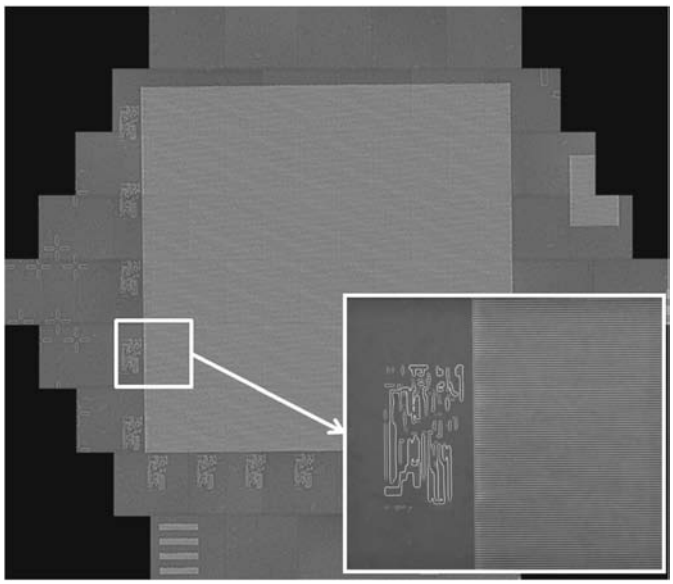

Figure 5: Semiconductor test sample with line patterns for metrology experiments. The imaged sample contains 60 nm amorphous silicon patterns on a 2 nm SiO_2 gate oxide. The features were patterned with 193 nm immersion lithography and dry-etched. The sample was coated with a thin conducting layer prior to imaging in the multi-beam SEM. Data acquisition rate: 0.26 GPixel/s at 3.8 nm pixel size, full hexagon width = 110 µm. Inset in lower right is a 12 µm × 10 µm single-beam sub-image detail of the full multi-beam image [27]. A possible Moiré pattern might be visible in the printed image that is due to binning effects of the image data. (Sample by SEMATECH).

Discussion

Image quality. The data indicate that the multi-beam SEM accommodates well the SNR versus throughput requirements mentioned above. The resolution of all sub-images in the tiled images (Figures 3–5) differs by only few percent, while contrast uniformity is even better. This demonstrates that the multi-beam SEM is a viable tool for these applications. The next step, providing large-scale data acquisition capabilities for the multi-beam SEM, requires a closer look at the automation of the data acquisition process.

Fine adjustments. Operating a multi-beam SEM resembles operating a single-beam SEM in many aspects. However, a multi-beam SEM requires a higher degree of automation during adjustment. Tasks that a human operator fulfills on a single-beam instrument for each image, such as focus, stigmation, and determination of exact imaging position, need to be automated for the multi-beam tool in order to avoid repeated time-consuming operator interaction. We illustrate this using beam pitch, that is, the relative distance between the electron beams at the sample. The illumination part of the multi-beam SEM electron optics contains a number of electron optical lenses. If a measurement of the relative distance between beams reveals that the beam pitch needs to be readjusted, changing the excitation of a single lens results not only in a change of beam pitch, but also in a change of focus at the sample. If that lens is a magnetic lens, the rotation of the beam positions around the central beam will change as well. This means that by adjusting one operational parameter, such as beam pitch, a number of other electron optical settings must be adjusted in concert. This is preferably done with

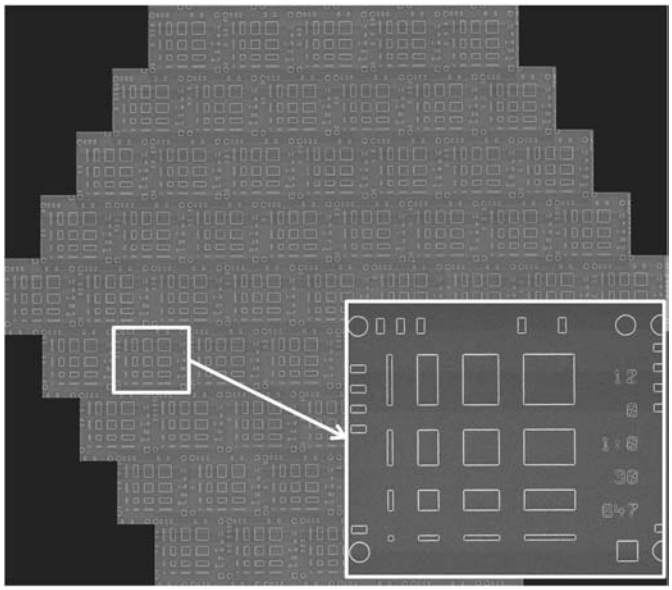

Figure 6: Test chip showing a hexagonal arrangement of calibration structures for adjustments to a multi-beam SEM. Sample was printed by an e-beam direct-write lithography process with high placement precision, etched in SiO_2 on a Si-substrate, and coated with a conductive layer. Data acquisition rate: 0.52 GPixel/s at 6 nm pixel size, full hexagon width = 110 µm. Inset in lower right is a 12 µm × 10 µm single-beam sub-image detail from the full multi-beam image.

an algorithm that operates on an appropriate test sample. Figure 6 shows an image of a multi-beam test wafer that contains test structures suitable for automated alignment and calibration of a multi-beam SEM.

Data generation. The maximum achievable data rate with the current multi-beam SEM, using 61 beams and a 20 MHz scanning rate, is about 100 TB per day. In a 91-beam configuration, this number increases to almost 160 TB per day. These figures do not take into account overhead times, such as stage movements, autofocus, fly-back times, etc. Because the current multi-beam setup has been optimized for a trade-off between cost and performance and has not been optimized for raw acquisition speed, these overhead times add to the scanning time, currently reducing the overall data rates by a factor of about two. It should be noted that solutions to significantly reduce these overhead times, such as faster stages, are already commercially available.

Data storage. For the operation of a multi-beam SEM, a strategy for storing and processing the data is paramount. If lossless storage of data is required, the availability of ample storage space at manageable cost seems to be ensured at least for the near future. It should be noted that data storage density has consistently been able to outpace Moore's law for many years [28]. Real-time compression of data will reduce the amount of storage space required. For lossless data compression, the compression factor will depend on the noise level present in the images [29]. If lossless data compression is not required, higher data compression rates are feasible. Ultimately, online image processing could provide further data compression for suitable applications by reducing the image information to a few performance indicators and discarding all image data except for those with performance indicators in a pre-set range.

Post-processing. For a number of applications, data post-processing is expected to be at least as time-consuming as data acquisition [30]. Work on image processing routines that aim to eliminate or at least minimize manual user interaction in the post-processing of large-volume data are in progress [31]. The continual development of semiconductor technology suggests that post-processing speed will keep up with the data acquisition speed.

Future developments. We expect the data volumes needed in the reconstruction of brain tissue will rise even beyond the example mentioned in the Introduction because future research directions already point toward reconstructing a whole brain with the aim of mapping its connectome, that is, the brain's wiring diagram [32]. One of the current model organisms, for example, is the mouse with a brain volume of approximately 500 mm^3. The multi-beam SEM is scalable to much higher beam numbers and total beam currents than demonstrated here in order to meet future needs. For example, these scalable improvements should open the door to investigations of macroscopic objects millimeters to centimeters in length with nm resolution [33]. It also enables a different approach to large-area sample work, as whole areas can be imaged at high resolution, and the sample sites of interest can be searched and identified on the data set rather than by searching and repeatedly scanning the sample itself. Thus, the sample would need to be scanned only once. In connection with the highly efficient detector setup, this means that electron beam damage can be minimized. This is advantageous for the imaging of beam-sensitive samples that are of high importance. An example would be critical dimension (CD) metrology or inspection on photoresist structures during semiconductor processing, where the electron beam illumination could cause changes in resist structures ("resist shrinkage").

Conclusions

Recent developments in three-dimensional imaging of tissue and inspection of wafers reveal a need for high-throughput, high-resolution electron microscopy, which we expect to be difficult to attain with current single-beam SEM technology. In this article we demonstrated the utility of multi-beam SEM images in two important application fields at high throughput and high quality, achieving remarkably shorter image acquisition times than possible with a single-beam SEM at comparable resolution. The multi-beam SEM employs a beam number and data acquisition concept that is scalable to permit even greater performance. This method is therefore positioned to meet future requirements in throughput and to incorporate future single-beam SEM enhancements.

Acknowledgements

The authors thank Tomasz Garbowski for the preparation of the images, and Ingo Müller, Stephan Nickell, Pascal Anger, Thomas Kemen, Nicole Rauwolf, and Gregor Dellemann for many insightful discussions.

References

[1] Carl Zeiss Microscopy, "JetSCAN The portable SEM for health monitoring of aircraft engines," *Carl Zeiss Microscopy*, 2012, http://www.zeiss.com/microscopy/en_us/products/scanning-electron-microscopes/tools/jetscan.html.
[2] V Drexel et al., *Proceedings MSA* (1994) 486–87.
[3] L Muray et al., *Proc SPIE* 9236 (2014) 92360C.
[4] L Reimer, *Scanning Electron Microscopy: Physics of Image Formation and Microanalysis*, 2nd completely rev. and updated ed., Springer, New York, 1998.
[5] S Redeann and T Müller-Reichert, *J Microsc* 251(2) (2013) 109–12.
[6] J Caplan et al., *Curr Opin Struct Biol* 21(5) (2011) 686–93.
[7] EA Smith et al., *Ultramicroscopy* 143 (2014) 33–40.
[8] JM Perkel, *BioTechniques* 57(4) (2014) 172–77.
[9] C Smith, *Nature* 492(7428) (2012) 293–97.
[10] OD Patterson et al., *Proc SPIE* 8324 (2012) 83242J.
[11] B Thiel et al., *Proc SPIE* 9236 (2014).
[12] J.-P. Kaiser et al., *PloS One* 8(12) (2013) e83215.
[13] SF Evans et al., *Biomaterials* 34(8) (2013) 1878–87.
[14] ML Knothe Tate, *J Biomech* 44(2) (2011) 304–12.
[15] JW Lichtman and W Denk, *Science* 334(6056) (2011) 618–23.
[16] M Helmstaedter et al., *Nature* 500(7461) (2013) 168–174.
[17] PS Holcomb et al., *J Neurosci Off J Soc Neurosci* 33(32) (2013) 12954–69.
[18] A Rose, *J Opt Soc Am* 38(2) (1948) 196.
[19] DS Bright et al., *J Microsc* 189(1) (1998) 25–42.
[20] GH Jansen, *Coulomb interactions in particle beams*, Academic Press, Boston, 1990.
[21] KL Briggman and DD Bock, *Curr Opin Neurobiol* 22(1) (2012) 154–61.
[22] W Denk and H Horstmann, *PLoS Biol* 2(11) (2004) e329.
[23] K Hayworth et al., *Microsc Microanal* 12(S02) (2006) 86–87.
[24] JC Tapia et al., *Nat Protoc* 7(2) (2012) 193–206.
[25] KJ Hayworth et al., *Front Neural Circuits* 8 (2014) 68.
[26] AL Eberle et al., "High-resolution, high-throughput imaging with a multibeam scanning electron microscope," *J Microsc* (2015) , Epub ahead of print (see also doi: 10.1111/jmi.12224).
[27] W Ito et al., *Proc SPIE* 9050 (2014) 90500D.
[28] C Walter, "Kryder's Law," *Scientific American*, July 25, 2005, http://www.scientificamerican.com/article/kryders-law.
[29] WH Press, ed., *Numerical Recipes: The Art of Scientific Computing*, 3rd ed., Cambridge University Press, New York, 2007.
[30] G Knott and C Genoud, *J Cell Sci* 126(20) (2013) 4545–52.
[31] JW Lichtman et al., *Nat Neurosci* 17(11) (2014) 1448–54.
[32] S Seung, *Connectome: How the Brain's Wiring Makes Us Who We Are*. Mariner Books. Houghton Mifflin Harcourt, Boston, 2013.
[33] V Marx, *Nature* 503(7474) (2013) 147–52.

MT

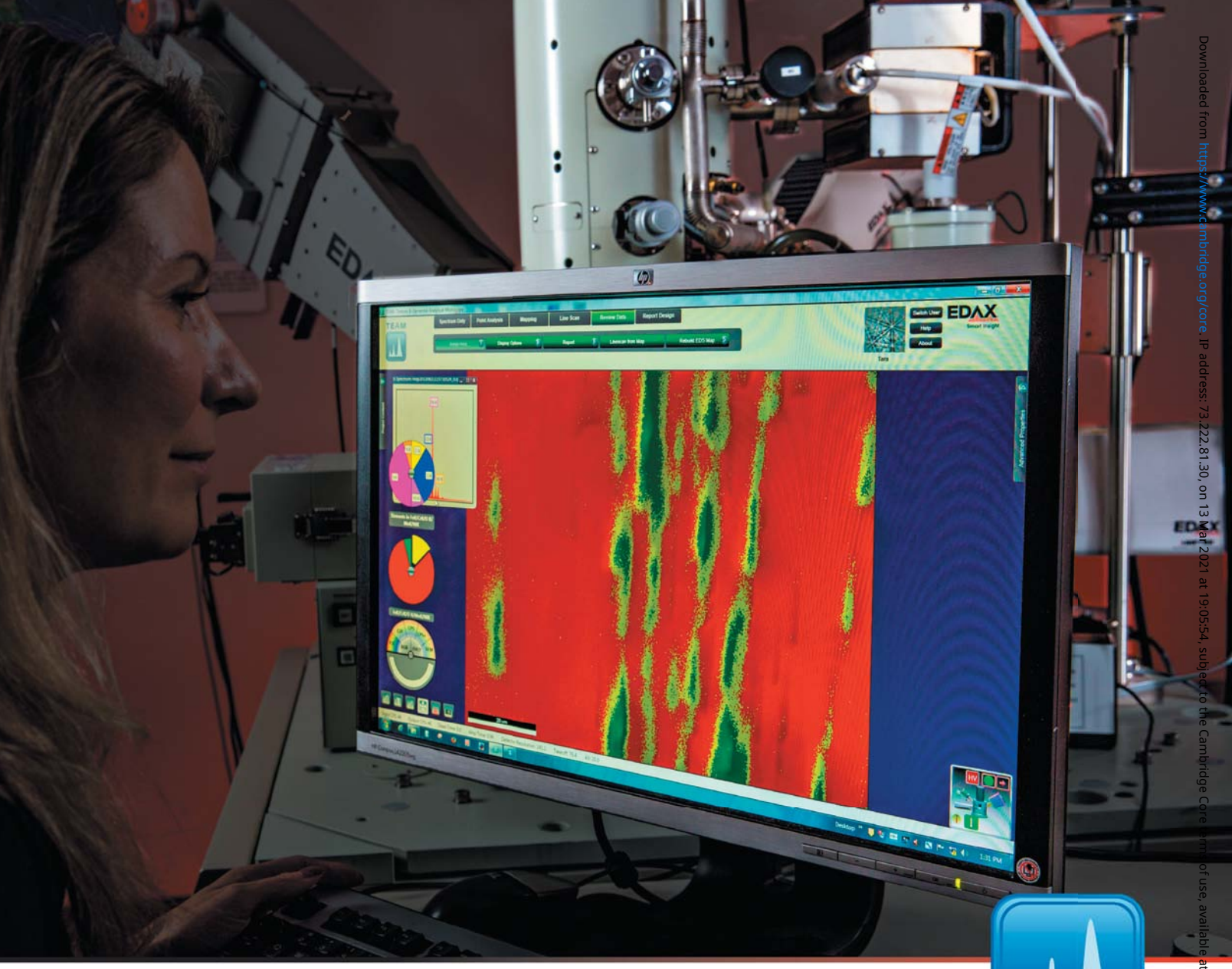

TEAM™ EDS

TEAM™ EBSD

TEAM™ WDS

Best resolution and highest throughput when results matter.

- Octane series SDDs with advanced electronics providing three times the throughput of a typical SDD
- Best resolution EDS data at previously unmatched speeds
- Intuitive and easy to use TEAM™ interface
- Fast data collection with high quality results
- Now available for both SEM and TEM

Power your next insight with EDAX.
edax.com/TEAM-EDS

AMETEK®
MATERIALS ANALYSIS DIVISION

EDAX®
Smart Insight